AIAA 81-0399R

Dynamic Simulation through Analytic Extrapolation

L.E. Ericsson* and J.P. Reding†
Lockheed Missiles & Space Company, Inc., Sunnyvale, Calif.

In spite of the rapid progress of computational fluid dynamics (CFD) the existing capability to predict full-scale missile dynamics is very limited. The main reason for this is the existing strong coupling between boundary-layer transition and vehicle motion, which cannot be simulated by present CFD methods and can be obtained experimentally only in tests at the full-scale Reynolds number. The present paper describes the interactive use of theoretical and experimental techniques to provide the means to "extrapolate analytically" to full-scale flight conditions. This capability is especially needed in regard to elastic vehicle dynamics because of the difficulties inherent in performing dynamic simulation of an elastic vehicle in the high Reynolds number ground testing facilities presently becoming available.

Nomenclature

c	= reference length, maximum chordwise extent for two-dimensional flow and maximum body diameter for three-dimensional flow
d	= body diameter
f	= oscillation frequency
l	= two-dimensional lift coefficient, $c_l = l/(\rho_\infty U_\infty^2/2)c$
L	= total body length
m_p	= two-dimensional pitching moment coefficient, $c_m = m_p/(\rho_\infty U_\infty^2/2)c^2$
M	= Mach number
M_p	= three-dimensional pitching moment coefficient, $C_m = M_p/(\rho_\infty U_\infty^2/2)(\pi/4)c^3$
N	= three-dimensional normal force coefficient, $C_N = N/(\rho_\infty U_\infty^2/2)(\pi/4)c^2$
p	= static pressure coefficient, $C_p = (p-p_\infty)/(\rho_\infty U_\infty^2/2)$
q	= pitch rate
Re	= Reynolds number, $Re_L = LU_\infty/\nu_\infty$
t	= time
U	= axial velocity
x	= axial distance from leading edge in two-dimensional flow and from nose tip in three-dimensional flow
α	= angle of attack
θ	= pitch perturbation, $\theta = \Delta\theta \sin\omega t$
θ_c	= cone half-angle
ν	= kinematic viscosity of air
ρ	= air density
ω	= angular oscillation frequency, $\omega = 2\pi f$

Subscripts

B	= base
CG	= center of gravity
max	= maximum
TR	= boundary-layer transition
W	= wall
∞	= freestream value

Derivatives

C_{mq}	$= \partial C_m/\partial(cq/U_\infty)$
$C_{m\dot{\alpha}}$	$= \partial C_m/\partial(c\dot{\alpha}/U_\infty)$
$C_{N\alpha}$	$= \partial C_N/\partial\alpha$
$C_{N\alpha x}$	$= \partial C_{n\alpha}/\partial x$
$\dot{\alpha}$	$= \partial\alpha/\partial t$

Introduction

IN subscale tests of wings it was customary to place a boundary-layer trip near the leading edge, thereby assuring turbulent flow over 90% or more of the downstream wing area. At high subsonic Mach numbers this old rule of thumb no longer works, as is demonstrated by experimental results[1] (Fig. 1). Using the trip to fix transition at the full-scale location results in too thick a boundary layer at the location of the shock that terminates the local supersonic flow region. As a consequence the flow separation occurs upstream of the full-scale location, causing large deviations in the aerodynamic characteristics. There is a similar problem on axisymmetric bodies[2] (Fig. 2).

It is in some cases possible to trip the boundary layer downstream of the full-scale transition location, thereby producing the correct boundary-layer thickness at the shock location.[3] Although this will give the correct static pressure distribution at $\alpha = 0$, it cannot give the correct aerodynamic derivatives as the transition is not allowed to respond to changes in the vehicle environment, e.g., through angle of attack (α) and angular rate ($q + \dot{\alpha}$). That this transition degree of freedom is important is well documented by experimental results, both in two- and three-dimensional flows.

The coupling between boundary-layer transition and model motion has especially large effects on the dynamic stability, resulting in the very restrictive requirement that dynamic tests have to be performed at full-scale Reynolds numbers in order to give a correct simulation of full-scale dynamics.[2,4] Although ground testing facilities are now becoming available which can achieve full-scale test Reynolds number,[5] they will all be very busy. Even if time were made available, it is not certain that elastic vehicle dynamic simulation will be possible.[6]

In spite of all the progress being made in computational fluid dynamics (CFD),[7] no one is presently ready to forecast when CFD simulation of the coupling between boundary-layer transition and vehicle motion will be possible. Thus, the vehicle dynamics present a special problem in preliminary design because in most cases the needed dynamic stability characteristics cannot be obtained by either theory or test

Presented as Paper 81-0399 at the AIAA 19th Aerospace Sciences Meeting, St. Louis, Mo., Jan. 12-15, 1981; submitted March 6, 1981; revision received Sept. 17, 1981.

*Senior Consulting Engineer. Associate Fellow AIAA.
†Staff Engineer. Associate Fellow AIAA.

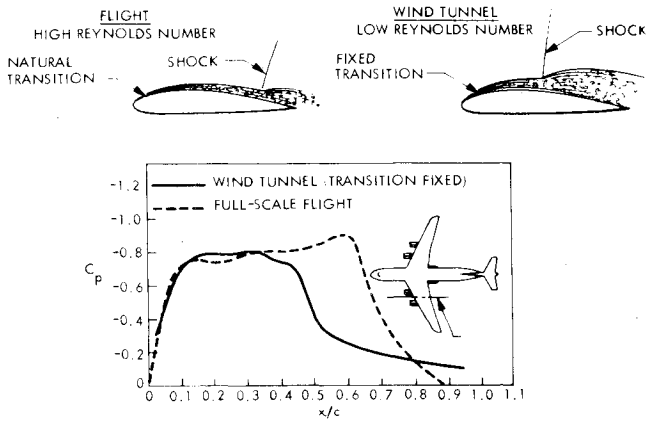

Fig. 1 Effect of boundary-layer tripping on shock-induced flow separation on an airfoil.[1]

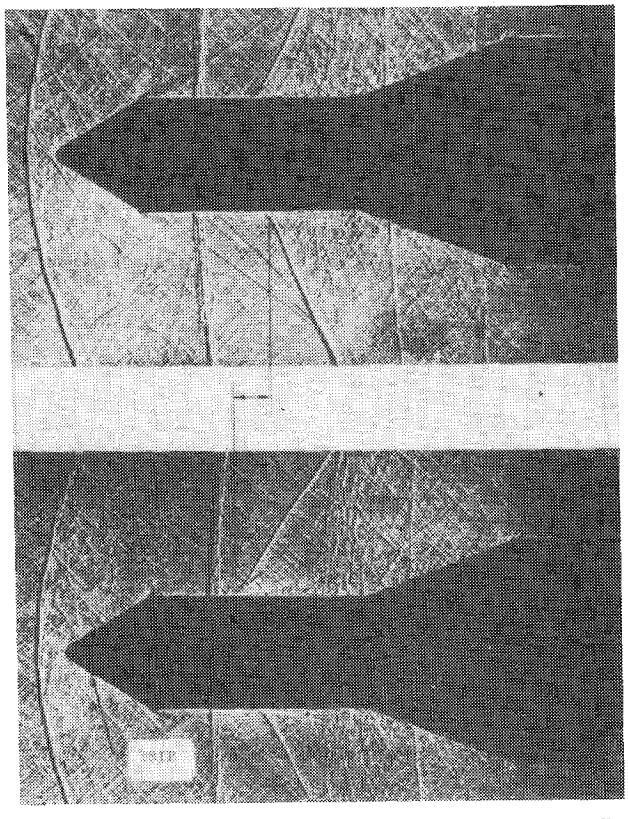

Fig. 2 Effect of boundary-layer tripping on flare-induced flow separation.

alone. The obvious solution to this dilemma is to use theoretical and experimental means in combination to provide dynamic simulation through analytic extrapolation, as will be described in the present paper.

Discussion

Various examples of transition effects on two-dimensional unsteady aerodynamic characteristics will be discussed first before going into the more complicated three-dimensional unsteady flow.

Two-Dimensional Flow

Figure 3 shows the phase characteristics measured for a 7.3% thick airfoil oscillating around the 22.7% chord.[8] When a trip wire was used to fix boundary-layer transition near the leading edge the measured phase (and amplitude) characteristics were in reasonably good agreement with in-

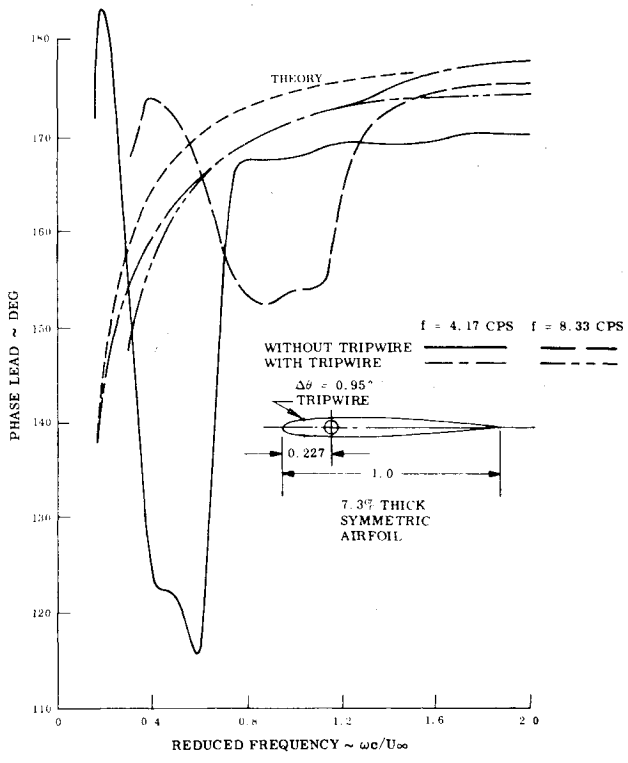

Fig. 3 Effect of boundary-layer transition on phase characteristics of an oscillating airfoil.[8]

viscid theoretical predictions. However, tests without a trip wire, which allowed the transition to respond to the airfoil motion, gave results that deviated greatly from the theoretical prediction.

In the test the reduced frequency $\omega c/U_\infty$ was changed by changing the wind-tunnel speed U_∞. Thus, the Reynolds number increases with decreasing reduced frequency. How the resulting forward movement of the transition can produce the observed anomalous phase (and amplitude) characteristics has been shown[9] by applying the analytic methods developed for dynamic trailing-edge stall.[10] These results indicate that the coupling between airfoil motion and boundary-layer transition will have a large effect on dynamic trailing-edge stall.[9,11]

A natural reaction by the design engineer to the results in Fig. 3 would be to point out that in full-scale flight transition does occur near the leading edge, questioning if not the coupling between transition and airfoil motion is much less of a problem in that case. The answer is "no." The coupling effects become even stronger, as is illustrated by the results in Fig. 4. It can be shown[12] that the large overshoot of static $c_{l\max}$ by the experimental data[13] is to a large extent (from $c_l = 1$ to 2) caused by the transition response to the airfoil pitch-up motion. The solid symbol at $c_l \approx 2$ in Fig. 4 is the overshoot predicted in Ref. 12 due to the moving-wall/wall-jet effect[14] (Fig. 5). The moving wall creates a wall-jet-like effect on the boundary-layer development between stagnation and flow separation points. It was postulated in Ref. 14 that this eliminated the laminar leading-edge bubble present in static stall, in the same manner as the blowing employed by Wallis,[15,16] thus explaining much of the large dynamic overshoot of static $c_{l\max}$. Experimental results by McCroskey et al.[17] later confirmed this dynamic elimination of the laminar leading-edge bubble. The last portion of the c_l overshoot in Fig. 4, $c_l > 2$, is the transient effect of a "spilled" leading-edge vortex, which becomes important only for high-frequency/large-amplitude oscillations.[12]

It was shown recently[18] that similar moving-wall/wall-jet effects on boundary-layer transition can account for the

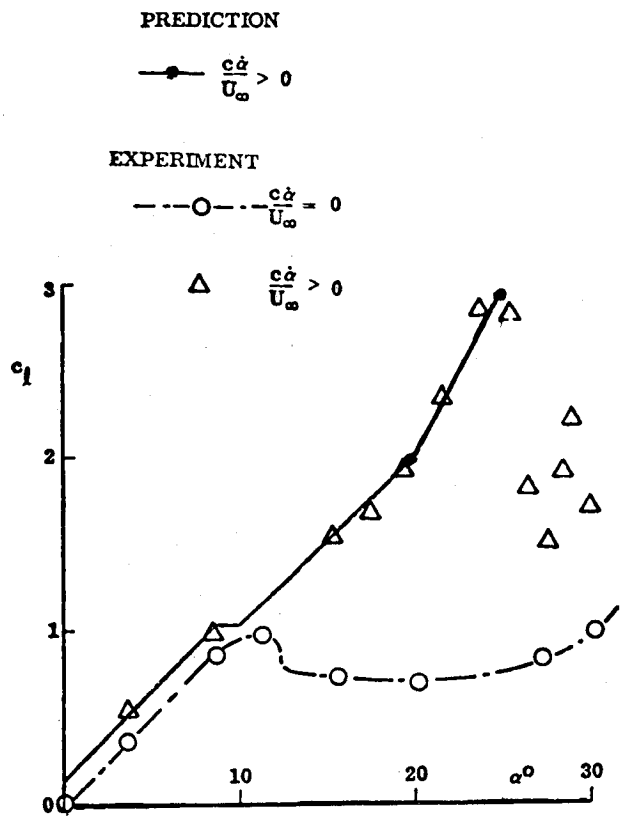

Fig. 4 Dynamic overshoot of static $C_{l_{max}}$.

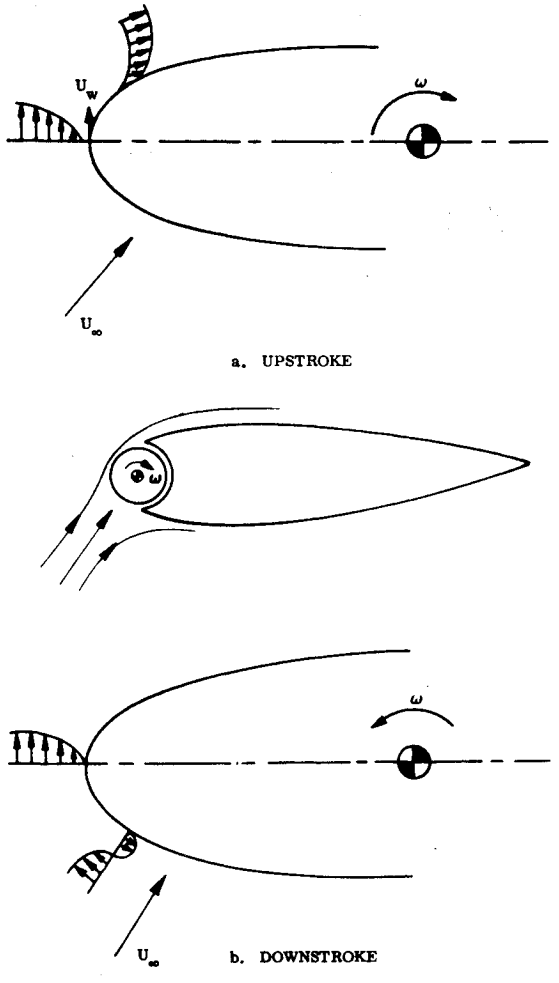

Fig. 5 Moving wall/wall jet analog for oscillating airfoil.

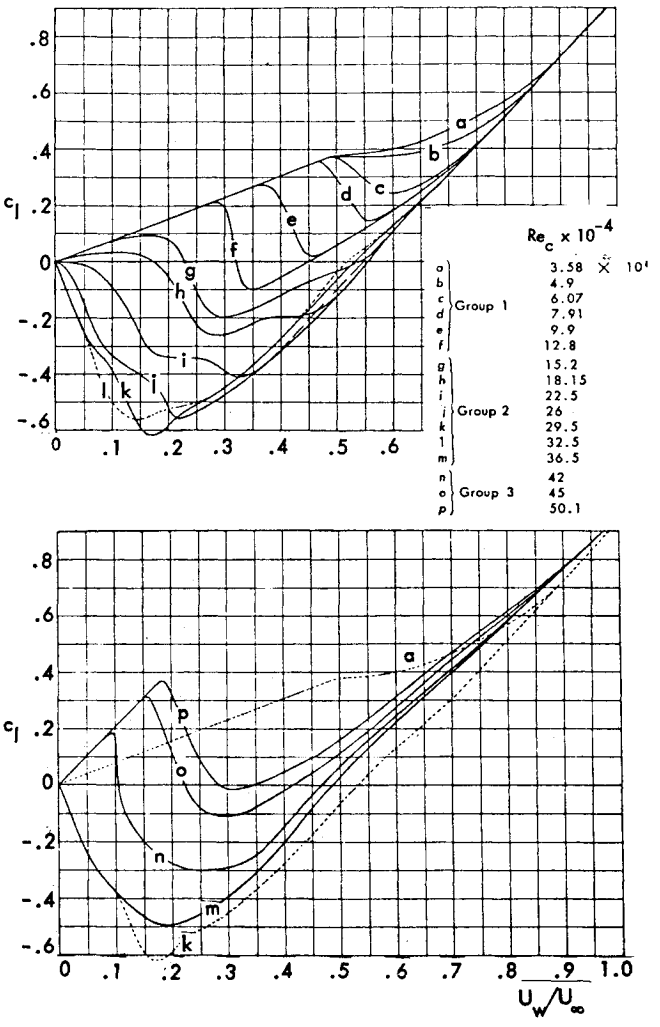

Fig. 6 Moving wall effect on the Magnus lift of a rotating circular cylinder.[19]

experimentally observed[19] reversal of the Magnus effect on a rotating circular cylinder (Fig. 6), as well as for the pitch-rate-induced change from supercritical to subcritical flow separations on an ogive cylinder body at high angles of attack[20,21] (Fig. 7). The reversal of the vortex-induced loads on coning axisymmetric bodies can also be shown to be caused by moving wall effects on boundary-layer transition and flow separation.[20]

Three-Dimensional Flow

On slender axisymmetric bodies the boundary-layer transition is very sensitive to angle-of-attack variations around $\alpha = 0$, as is illustrated by the sharp-cone data[22] in Fig. 8. Transition moves forward 50% of the body length on the leeward side of a 10 deg cone, when the angle of attack is increased from $\alpha = 0$ to 2 deg (Fig. 8a). This is caused by three-dimensional crossflow effects, which in the dynamic case lag the vehicle motion, explaining how the transition has opposite effects on static and dynamic stability[23,24] (Fig. 8b).

Transition effects are seen to increase the cone damping by 30% (Fig. 8b) and to have an equally large effect on the damping of an ogive cylinder body[25] (Fig. 9). It is shown in Ref. 26 how such transition-induced effects increased the inviscid transonic damping[27] of a 5 caliber ogive cylinder body by 50% (Fig. 10a). The empirical design code based upon this and similar experimental data, the so-called Spinner code, overpredicts by 100% the damping of a 3 caliber ogive cylinder body, which is too short to experience any transition effects (Fig. 10b). When the leeside transition front moves

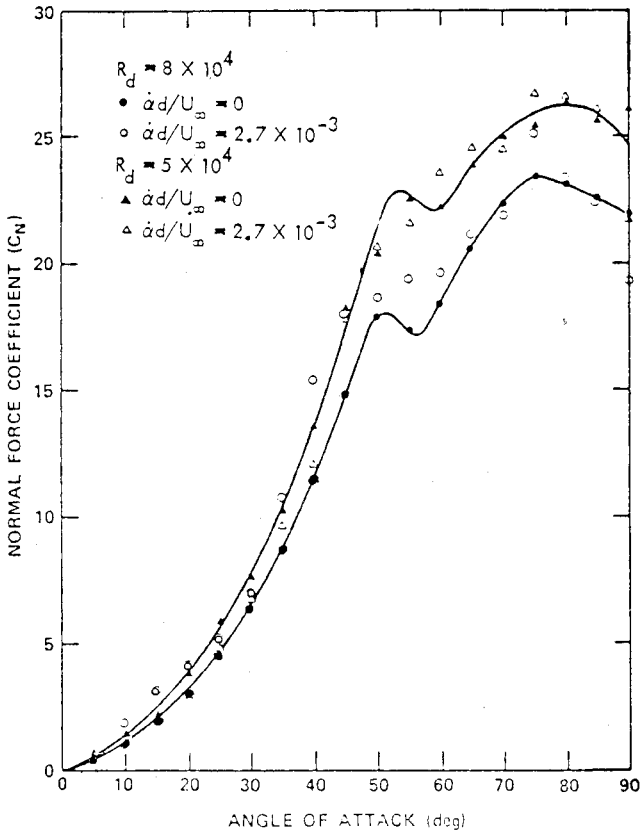

Fig. 7 Effect of pitch rate on the normal force of a slender ogive cylinder.[21]

forward of the rotation axis the effects on stability characteristics are reversed, exemplified by the static stability effects on a 10 deg cone[24] (Fig. 11). (The large amplitude, $\Delta\theta = \theta_c/3$, explains why $x_{TR}/L > 1$ for $\alpha = 0$.) The decreased dynamic stability of a cone-cylinder[28] (Fig. 12) could be caused by forebody transition effects, amplified by flow separation effects at transonic speed.[26] The results in Figs. 11 and 12 illustrate the problem of scaling subscale dynamic test data to full-scale Reynolds number. The transition may occur on the aft body in the test and could give a very unconservative value of the dynamic stability, especially if flow separation is also occurring on the body.

Analytic Extrapolation

When the aerodynamic loads are generated by attached flow, there are time-proven theoretical methods[29,30] by which the aeroelastic response of aircraft, missiles, and space vehicles can be determined. However, in many cases, especially in regard to missiles and aerospace launch vehicles, aerodynamic considerations rarely have any decisive impact on the design. As a result those vehicles often have large regions of separated flow, as is exemplified by the Saturn-Apollo rocket (Fig. 13a), and the aerodynamic loads are dominated by separated flow (Fig. 13b). In spite of the progress that is constantly being made, no satisfactory theoretical method is yet available whereby these separated flow effects can be predicted. Thus, they have to be determined experimentally, as in the case shown in Fig. 13.

The experimental static load distribution can be used directly in an aeroelastic analysis to determine the static divergence characteristics of the structure. However, to determine the dynamic structural response requires knowledge of the unsteady aerodynamic loads. For an elastic vehicle, such as the Saturn-Apollo launch vehicle, these loads can be determined experimentally only through tests in which the elastic vehicle dynamics are fully simulated.[31] Because of

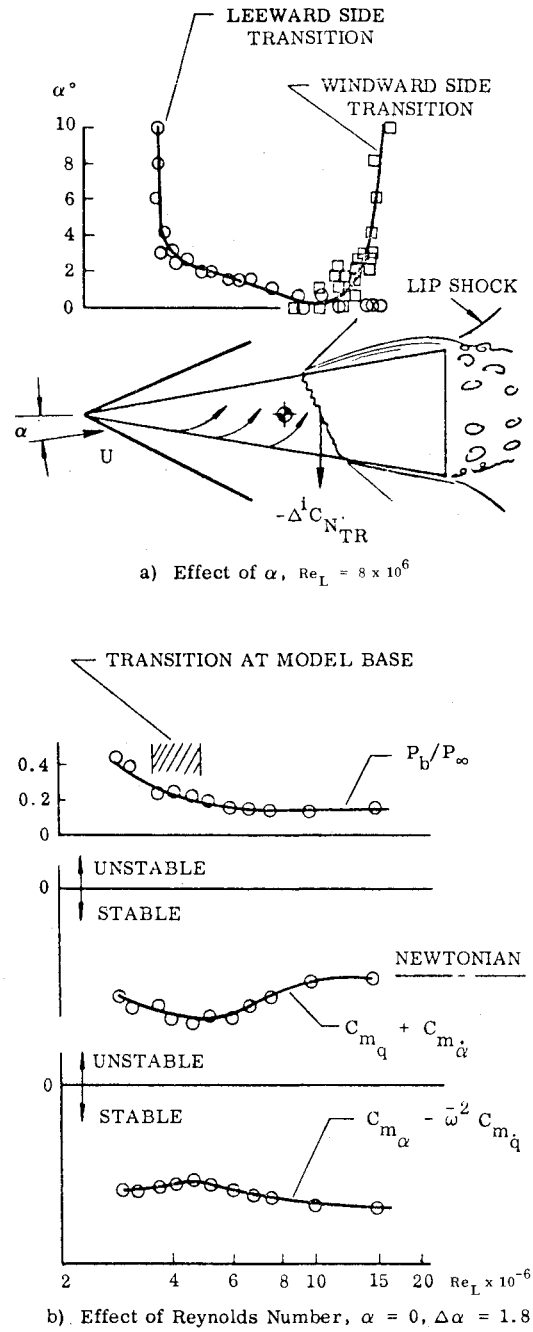

Fig. 8 Boundary-layer transition characteristics for a 10 deg sharp cone.[22]

the complexity of such a test the model design has to be "frozen" six or more months before the test. During this time period the full-scale vehicle design rarely remains "frozen." In the case of the Saturn-Apollo booster, its structure, geometry, and design trajectory had all changed significantly when the dynamic test data[31] finally became available. Without an analytic extrapolation method in which the effects of these changes could be accounted for, the test data could not be used to determine the dynamic response of the full-scale vehicle.

The key feature in the analytic extrapolation method developed for the Saturn-Apollo[32] was the use of static experimental data to obtain the unsteady aerodynamic loads. This could be done only by understanding fully the static separated flow effects and the dependence of the various separation-induced loads on the flow conditions on the forebody. The loads occurring in a separated flow region fall into two categories: 1) loads which depend only upon the

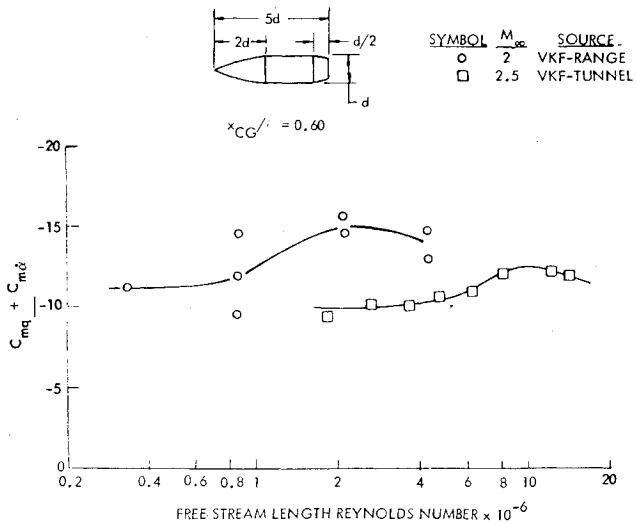

Fig. 9 Transition effects on the pitch damping of a 5 caliber ogive cylinder body.[25]

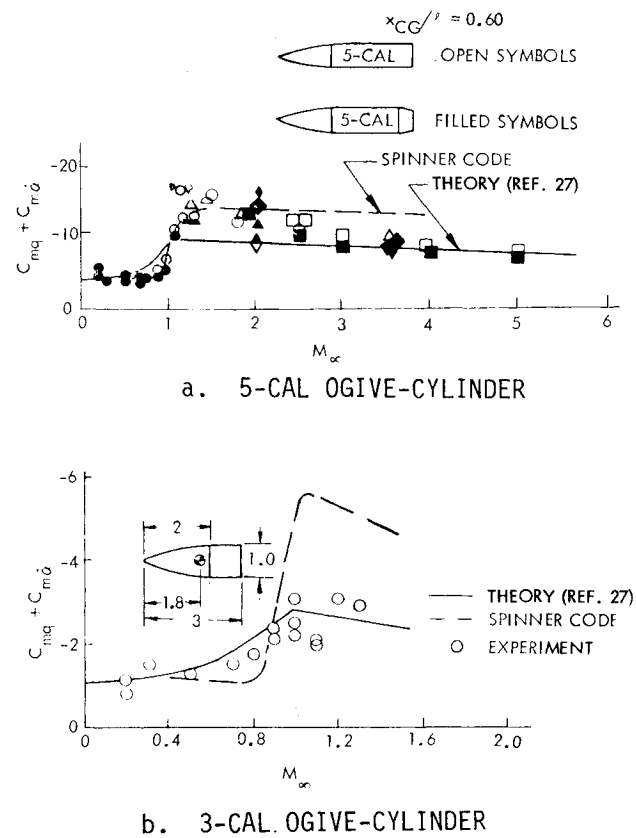

Fig. 10 Transition-induced distortion of predicted damping.[26]

instantaneous local flow conditions, and 2) the separation-induced load which is dependent upon the effect of forebody attitude and relative displacement on the flow separation. In the latter case there is a time lag before the forebody perturbation has altered the flow separation and the associated load on the submerged body element. The determination of this time lag and the differentiation between local and separation-induced loads are the critical elements in the analytic extrapolation method. Various checks are needed before one can be satisfied that the method can predict the full-scale characteristics with the needed accuracy. The steps taken to insure the accuracy of the Saturn-Apollo method[32] will be described before outlining a more general method

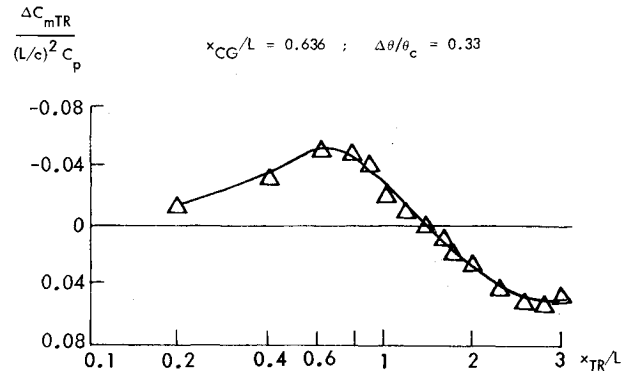

Fig. 11 Reversal of transition-induced effects on sharp-cone stability characteristics.[24]

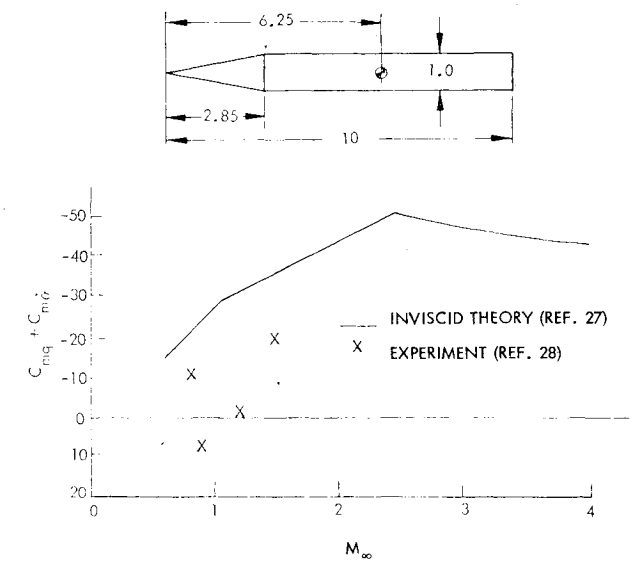

Fig. 12 Viscosity-induced adverse damping effects on a cone cylinder body.

which includes dynamic simulation of the coupling between boundary-layer transition and vehicle motion.

Figure 14 shows the static load distribution and the corresponding damping distribution for the second bending mode of the Saturn-Apollo launch vehicle. Significant negative damping is generated by the Apollo command module, submerged in the wake from the escape rocket. Thus, this part of the prediction needed to be checked especially carefully. This was done in two ways. Rigid body damping of the escape configuration was investigated, showing that the experimentally observed negative damping[33,34] could be predicted (Fig. 15) by the same analytic method that gave the results shown in Fig. 14. Also the elastic partial mode simulation of the forward portion of the Saturn-Apollo vehicle[35] gave experimental results (Fig. 16) that were in good agreement with the analytic prediction. Consequently, the good agreement between analytic predictions[32] and elastic vehicle experimental results[31] shown in Fig. 17 led to the conclusion that the analytic extrapolation method[32] was accurate enough to be the sole tool used to predict the aeroelastic characteristics for all the following Saturn-Apollo configurations.[36]

In the case of the Saturn-Apollo launch vehicle the critical flow separation, the escape rocket wake, was fixed by the geometry and boundary-layer transition simulation was not necessary for successful analytic extrapolation of subscale experimental results. In the many cases where boundary-layer transition plays a significant role, one has to go through the

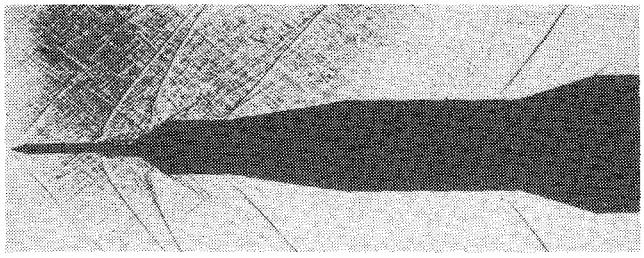

a)

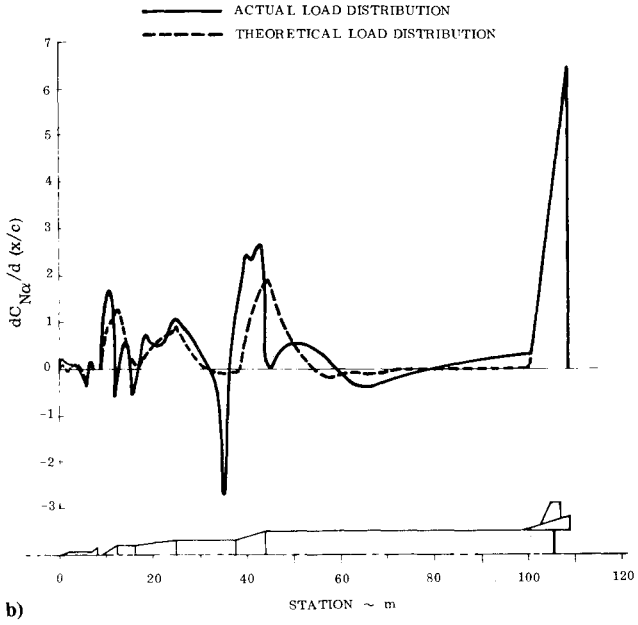

b)

Fig. 13 Effect of flow separation on Saturn-Apollo launch vehicle: a) separated flow regions and b) load distribution.

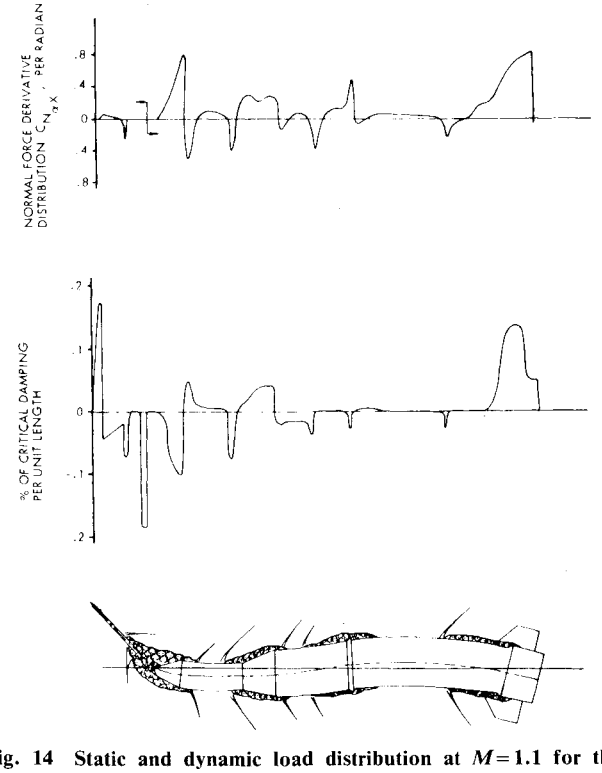

Fig. 14 Static and dynamic load distribution at $M=1.1$ for the second bending mode of the Saturn I-Apollo launch vehicle with disk-on escape rocket.[32]

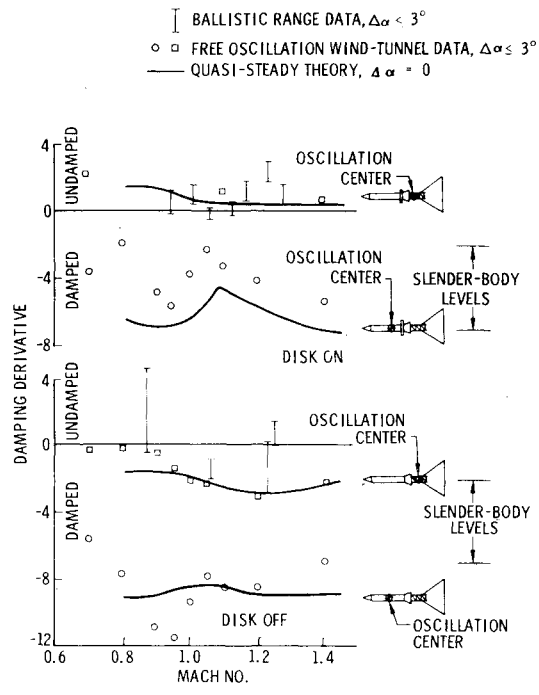

Fig. 15 Comparison between predicted and measured pitch damping of the Saturn-Apollo escape configuration.[32]

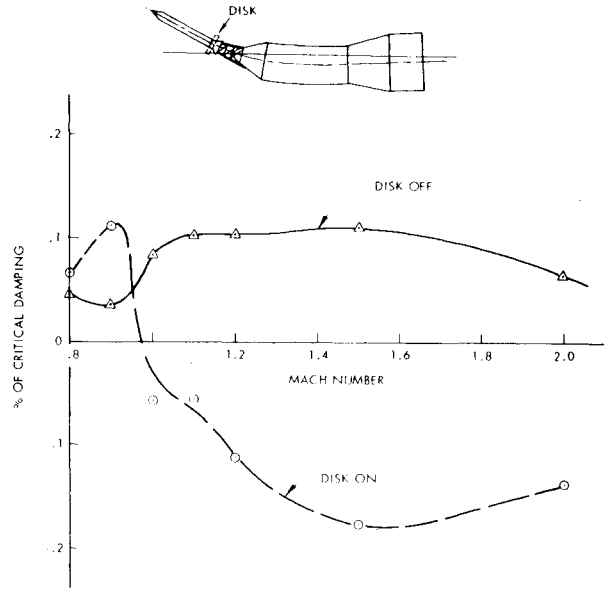

Fig. 16 Forebody damping for the second bending mode of the Saturn-Apollo launch vehicle.

following steps:

1) Establish analytic relationships between dynamic and static aerodynamic characteristics for the same subscale Reynolds number, and check the veracity of the analytic predictions against dynamic test data.

2) Determine experimentally the effect of Reynolds number on the static aerodynamic characteristics from the subscale Reynolds numbers of the dynamic test up to full-scale Reynolds number.

3) In many cases it may be possible to verify the analytic extrapolation to full-scale Reynolds numbers by dynamic rigid body tests, simulating a critical portion of the elastic vehicle dynamics, as in the case of the escape configuration (Fig. 15) for the Saturn-Apollo elastic vehicle dynamics (Figs. 14 and 17).

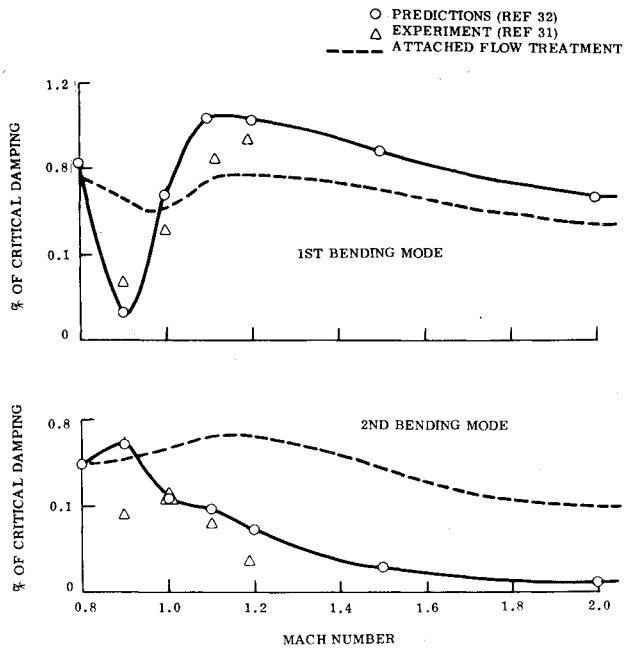

Fig. 17 Comparison between predicted and measured aeroelastic stability characteristics of the Saturn I-Apollo launch vehicle with disk-on escape rocket.

Conclusions

A review of the scaling problem in dynamic tests has revealed the following:

1) A key element in dynamic simulation, the strong coupling between boundary-layer transition and vehicle motion, cannot be simulated in experiments at subscale Reynolds numbers nor can it be simulated by existing theoretical methods.

2) It may often not be possible to simulate full-scale elastic vehicle dynamics in dynamic tests performed at full-scale Reynolds numbers.

3) A solution to this dilemma is to provide dynamic simulation through analytic extrapolation using static experimental data obtained at subscale and full-scale Reynolds numbers, together with selected rigid body dynamic data, usually obtained only at subscale Reynolds numbers.

References

[1] Loving, D.L., "Wind-Tunnel-Flight Correlation of Shock-Induced Separated Flow," NASA TN D-3580, 1966.

[2] Ericsson, L.E. and Reding, J.P., "Reynolds Number Criticality in Dynamic Tests," AIAA Paper 78-166, Jan. 1978.

[3] Blackwell, J.A. Jr., "Preliminary Study of Effects of Reynolds Number and Boundary Layer Transition Location on Shock-Induced Separation," NASA TN D-5003, Jan. 1969.

[4] Ericsson, L.E. and Reding, J.P., "Scaling Problems in Dynamic Tests of Aircraft-Like Configurations," Paper 25, AGARD-CP-227, Sept. 1977, pp. 25-1-25-11.

[5] Howell, R.R. and McKinney, L.W., "The US 2.5 Meter Cryogenic High Reynolds Number Tunnel," Paper presented at 10th ICAS Congress, Ottawa, Canada, Oct. 1976.

[6] *Workshop of High Reynolds Number Research*, NASA SP-2009, Oct. 1976.

[7] Chapman, D.R., "Dryden Lecture: Computational Aerodynamics Development and Outlook," *AIAA Journal*, Vol. 17, Dec. 1979, pp. 1293-1313.

[8] Greidanus, J.H., Van de Vooren, A.I., and Bergh, H., "Experimental Determination of the Aerodynamic Characteristics of an Oscillating Wing with Fixed Axis of Rotation," NLL Rept. F101, Jan. 1952.

[9] Ericsson, L.E. and Reding, J.P., "Dynamic Stall of Helicopter Blades," *Journal of American Helicopter Society*, Vol. 17, Jan. 1972, pp. 10-19.

[10] Ericsson, L.E. and Reding, J.P., "Unsteady Airfoil Stall Review and Extension," *Journal of Aircraft*, Vol. 8, Aug. 1971, pp. 609-616.

[11] Ericsson, L.E. and Reding, J.P., "Dynamic Stall Analysis in Light of Recent Numerical and Experimental Results," *Journal of Aircraft*, Vol. 13, April 1976, pp. 248-255.

[12] Ericsson, L.E. and Reding, J.P., "Dynamic Stall at High Frequency and Large Amplitude," *Journal of Aircraft*, Vol. 17, March 1980, pp. 136-142.

[13] Ham, N.D. and Garelick, M.S., "Dynamic Stall Considerations in Helicopter Rotors," *Journal of American Helicopter Society*, Vol. 13, April 1968, pp. 44-55.

[14] Ericsson, L.E. and Reding, J.P., "Analytic Prediction of Dynamic Stall Characteristics," AIAA Paper 72-682, June 1972.

[15] Wallis, R.A., "Boundary Layer Transition at the Leading Edge of Thin Wings and Its Effect on General Nose Separation," *Advances in Aeronautical Sciences*, Proceedings of the Second International Congress in the Aeronautical Sciences, Zurich, Sept. 1979, pp. 161-184.

[16] Wallis, R.A., "The Turbulent Boundary Layer on the Articulated Nose of a Thin Wing Provided with Air Jets," Aeronautical Research Laboratories (Australia) Aero Note 141, Oct. 1954.

[17] McCroskey, W.J., Carr, L.W., and McAllister, K.W., "Dynamic Stall Experiments on Oscillating Airfoils," *AIAA Journal*, Vol. 14, Jan. 1976, pp. 57-63.

[18] Ericsson, L.E., "Karman Vortex Shedding and the Effect of Body Motion," *AIAA Journal*, Vol. 18, Aug. 1980, pp. 935-944.

[19] Swanson, W.M., "The Magnus Effect: A Summary of Investigations to Date," *Journal of Basic Engineering*, Vol. 83, Sept. 1961, pp. 461-470.

[20] Ericsson, L.E. and Reding, J.P., "Steady and Unsteady Vortex-Induced Asymmetric Loads on Slender Vehicles," *Journal of Spacecraft and Rockets*, Vol. 18, March-April 1981, pp. 97-109.

[21] Smith, L.H., "Aerodynamic Characteristics of an Axisymmetric Body Undergoing a Uniform Pitching Motion," Ph.D. Thesis, Naval Postgraduate School, Monterey, Calif., Dec. 1974.

[22] Ward, L.K., "Influence of Boundary Layer Transition on Dynamic Stability at Hypersonic Speeds," *Transactions of the Second Technical Workshop on Dynamic Stability Testing*, Vol. II, Paper 8, AEDC, Arnold Air Force Station, Tenn., April 1965.

[23] Ericsson, L.E., "Effect of Boundary Layer Transition on Vehicle Dynamics," *Journal of Spacecraft and Rockets*, Vol. 6, Dec. 1969, pp. 1404-1409.

[24] Ericsson, L.E., "Transition Effects on Slender Vehicle Stability and Trim Characteristics," *Journal of Spacecraft and Rockets*, Vol. 11, Jan. 1974, pp. 3-11.

[25] Ward, L.K., Private communication of unpublished experimental results, Feb. 1972.

[26] Ericsson, L.E., "Viscous Effects on Missile Aerodynamics at Low Angles of Attack," *Journal of Spacecraft and Rockets*, Vol. 18, Sept.-Oct. 1981, pp. 401-405.

[27] Ericsson, L.E., "Effect of Mach Number on Slender Vehicle Dynamics," *Journal of Spacecraft and Rockets*, Vol. 18, Jan.-Feb. 1981, pp. 18-23.

[28] Murphy, C.H., "Free Flight Motion of Symmetric Missiles," BRL Rept. 1216, July 1963.

[29] Bisplinghoff, R.L., Ashley, H., and Halfman, R.L., *Aeroelasticity*, Addison-Wesley Publishing Co., Reading, Mass., 1955.

[30] Bisplinghoff, R.H. and Ashley, H., *Principles of Aeroelasticity*, John Wiley and Sons, New York, 1962.

[31] Hanson, P.W. and Dogget, R.V. Jr., "Wing Tunnel Measurements of Aerodynamic Damping Derivatives of Launch Vehicle Vibrating in Free-Free Bending Modes at Mach Numbers From 0.7 to 2.87 and Comparison With Theory," NASA TN D-1391, 1962.

[32] Ericsson, L.E. and Reding, J.P., "Analysis of Flow Separation Effects on the Dynamics of a Large Space Booster," *Journal of Spacecraft and Rockets*, Vol. 2, July-Aug. 1965, pp. 481-490.

[33] Lowndes, R.I. and Shadow, T.U., "Transonic Static and Dynamic Stability of Several Saturn IB and V Upper Stage Configurations," AEDC TR-66-125, June 1966.

[34] Unpublished ballistic range data obtained at Ballistic Research Laboratories, Aberdeen, Md., 1966.

[35] Cole, H. Jr., Robinson, R., and Gambucci, B., "Buffeting Response of the Apollo Partial Mode Model at Subsonic and Supersonic Mach Numbers," NASA TN D-2689, Feb. 1965.

[36] Rainey, A.G., "Progress in the Launch Vehicle Buffeting Problem," *Journal of Spacecraft and Rockets*, Vol. 2, May-June 1965, pp. 289-299.